Hindawi
Geofluids
Volume 2023, Article ID 4445749, 14 pages
https://doi.org/10.1155/2023/4445749

Research Article

Diagenetic Facies and Their Controls on the Quality of Tight Sandstone Reservoirs: A Case Study from the Upper Paleozoic Gas Reservoir in the Eastern Ordos Basin, North China

Xiaoli Qin,[1,2] **Rongxi Li**,[1,2] **Lei Chen**,[3] **Kun Jiao**,[4] **Jinghua Cheng**,[1,2] **Ahmed Khaled**,[1,2] **Limiao Yao**,[5] **and Junnian Chen**[6]

[1]*School of Earth Sciences and Resources, Chang'an University, Xi'an 710054, China*
[2]*Key Laboratory for the Study of Focused Magmatism and Giant Ore Deposits, MLR, Xi'an 710054, China*
[3]*Shandong Provincial Key Laboratory of Deep Oil and Gas, China University of Petroleum (East China), Qingdao 266580, China*
[4]*State Key Laboratory of Oil and Gas Reservoir Geology and Exploitation, Chengdu University of Technology, Chengdu 610500, China*
[5]*Research Institute of Petroleum Exploration & Development, PetroChina, Beijing 100083, China*
[6]*Exploration & Development Research Institute of Liaohe Oilfield Company, Panjin 124010, China*

Correspondence should be addressed to Lei Chen; chenlei19880804@163.com

Received 23 December 2022; Revised 3 February 2023; Accepted 9 April 2023; Published 23 May 2023

Academic Editor: Jinze Xu

Diagenetic facies play a significant role in the evaluation and prediction of reservoirs as they comprehensively reflect the spatial distribution characteristics of deposition, diagenesis, and petrophysical properties. Based on the petrographic observation and considering pores, lithology, and diagenesis types, the diagenetic facies types were identified, and the pore evolution process and its influence on the quality of low permeability tight gas reservoirs were analyzed. The results show that six types of diagenetic facies were identified, including siliceous cementation intergranular pore facies (A), carbonate dissolution pore facies (B), matrix dissolution pore facies (C), clastic dissolution pore facies (D), matrix filling and strong compaction tight facies (E), and carbonate cementation and metasomatism tight facies (F). The evolution process of porosity shows that the restored original porosity is indicated to be between 34.2% and 36.0%. The average porosity loss caused by compaction was 17.1%, while the average porosity loss caused by cementation is 14.1%. The average porosity increased by 2.5% on diagenetic facies B, C, and D due to dissolution. Consequently, diagenetic facies A with weak compaction and diagenetic facies B, C, and D with strong dissolution are effective reservoirs with porosity greater than 6.6% and permeability greater than $(0.25 - 0.6) \times 10^{-3}$ μm^2. The distribution areas of A, B, C, and D are favorable areas for tight gas exploration and are important indicators for the prediction of tight gas in the Upper Paleozoic Shanxi Formation in the eastern Ordos Basin. This study provides a new petrographic method for reservoir prediction and exploration of natural gas, which has practical value and economic significance.

1. Introduction

Tight gas resources are distributed widely and have large reserves, making up an increasing proportion of the overall natural gas production. Additionally, their reserves and development potential are still enormous, which has significant strategic implications [1–4]. Numerous studies have found that the petrophysical properties of tight sandstone reservoirs are not "congenitally tight," with the recovery of the original porosity of sandstone showing that the petrophysical properties are good. Late diagenesis, specifically strong compaction, multiphase cementation, and the formation of authigenic minerals, causes the primary pore to become jammed and the reservoir to become tight [5, 6]. Exploration practice proved that tight clastic reservoirs basically show the five lowness characteristics of low porosity, low permeability, low abundance, low pressure, and low yield, which are mainly due to the strong heterogeneity of

reservoirs, including lithologic heterogeneity (interlayer, the quick lateral change of thickness) and petrophysical properties (porosity, permeability, and rock mechanics properties) [7]. The late diagenesis and the primitive sedimentary facies are the main causes of this heterogeneity. Among them, the spatial distribution of sand bodies and its original physical characteristics were determined by sedimentary facies, whereas diagenesis had an impact on the postpetrophysical properties [6, 8–11].

The results of reservoir evaluation based on the experimental analysis data of drilling core samples are difficult to reflect the actual situation of the plane and profile distribution of tight reservoirs with strong heterogeneity due to the limitations of core sampling sections, sample representativeness, and experimental methods. Sedimentary facies, which represent the reservoir petrology, diagenesis, and physical characteristics, are comprehensive reflections of diagenetic facies, diagenetic environment, and late diagenesis as a parameter of reservoir description. Therefore, diagenetic facies have been widely used by scholars around the world in the fields of oil and gas exploration and development, including studying pore structure, pore evolution characteristics, reservoir evaluation, prediction of high-quality reservoirs, and the study of the relationship between rock mechanics [12–14].

In the northern part of the Ordos Basin, several large-scale natural gas fields have been found in sand bodies of the Upper Paleozoic fluvial delta, which are distributed from the north to the south of the basin. Moreover, the explored natural gas reserves in the Upper Paleozoic fluvial delta sand bodies reached 8.4×10^{12} m^3 [15, 16]. Several large gas fields have been discovered along the Upper Paleozoic fluvial delta channel sand bodies in the eastern Ordos Basin in the past few years, which have proven reserves exceeding one trillion cubic meters of natural gas. Gas-bearing layers have been found in the Upper Paleozoic Shiqianfeng Formation (P3sh), Upper Shihezi Formation (P2sh), Lower Shihezi Formation (P2x), Shanxi Formation (P1s), Taiyuan Formation (P1t), and Benxi Formation (C2b), showing good exploration potential [15]. However, a large number of studies have shown that the Upper Paleozoic sandstone bodies in the eastern Ordos Basin are elongated and overlaid. The width, thickness, lithos, and physical property of delta channel sandstone bodies change rapidly. The gas reservoirs are characterized by low porosity, low permeability, low gas abundance, and low pressure, with complex cement minerals of sandstone and poor physical property. The heterogeneity of lithos, physical property, and even sensitivity of reservoir bed are strong, with diverse factors affecting petrophysical properties. As a result of strong tectonic uplift from the Late Cretaceous, the burial depth of the Upper Paleozoic strata is relatively shallow. However, the sandstones are subjected to strong diagenetic transformation resulting in the low permeability tight sandstone gas reservoir. There are few residual primary intergranular pores, and secondary dissolution pores are the main reservoir space. The reservoir has strong microscopic heterogeneity, low porosity, low permeability, small pore throat, and complex pore throat structure. Therefore, it restricts the further exploration of natural gas in the eastern basin [17, 18].

In this study, based on the petrographic observation and considering pores, lithology, and diagenesis types, the diagenetic facies types were identified, and the pore evolution process and its influence on the quality of low permeability tight gas reservoirs were analyzed. The zone of sandstone bodies with relatively higher porosity and higher permeability was favorable areas according to the beneficial diagenetic facies. This study provides a new petrographic method for reservoir prediction and exploration of natural gas, which has practical value and economic significance.

2. Geological Features

The Ordos Basin is an important part of the North China Block (NCB). The NCB evolved from the Archean and Early Proterozoic crystalline basement and has experienced the Late Proterozoic to Early Paleozoic marine carbonate platform evolution stage, Late Paleozoic epicontinental sea, and continental coal-bearing depositional evolution stages, forming a typical large inland lake until Mesozoic [19–21]. Regional tectonic evolution shows that the Ordos Basin is an important component of the stable north China craton from the Neoproterozoic to the Early Paleozoic. The Qinling Orogenic Belt was formed due to the South China Block moving northward and colliding with the NCB during the Hercynian to Early Indosinian period. In this process, the Ordos area located in the NCB was subjected to the north-south tectonic extrusion, and regional long-term uplift occurred. The Ordos Basin has been subjected to 150 million years of denudation and loss of the Late Ordovician to Early Carboniferous sedimentary until it deposited again in the Late Carboniferous. The marine sedimentary transformed to terrestrial facies, and thick coal-bearing sediments of alternative sea and river facies formed. The hydrocarbon source rocks and a thick layer of fluvial facies sandstone reservoir were well developed, constituting the broad source-reservoir-cap assemblage, which is the most important natural gas-producing layer in the Ordos Basin. During the Late Indosinian to Late Yanshan periods, the Paleo-Pacific plate was subducted to the Asian plate. The entire eastern part of China was uplifted, and the western Ordos Basin subsided and formed a large lake known as the Ordos large lacustrine basin, which resulted in the formation of an important oil-bearing system in China at present [21–24]. The Pacific plate accelerated subduction to Asia during the Late Middle Jurassic to Early Cretaceous, resulting in the collision of Pal-Asia and the western Pacific continent. Under the regional squeezing of NW trending, the eastern Ordos Basin was uplifted as a whole, and a gentle monocline structure with west dipping in the eastern part of the Ordos basin was formed. In addition, the research area in the eastern part of the Shanbei slope also becomes a monocline with a general inclination to the west. During the Late Yanshan to Himalayan periods, NV-SE stretching occurred in the Ordos Basin and a series of fault basins formed around the basin. The late tectonic activities had a certain impact on the early oil and gas accumulation in the Ordos Basin [24–27].

The sedimentary thickness of the Shanxi Formation in the east of the Ordos Basin is generally 80-140 m, with an

average thickness of about 100 m. The lithology is mainly gray medium-coarse-grained sandstone, siltstone, and mudstone, with multiple coal seams are developed. It is important coal-bearing system and natural gas-producing in the Ordos Basin, and the coal seams are important gas source rock [28, 29]. The Shanxi Formation is divided into Shan2 member and Shan1 member from bottom to top, among which the Shan2 member is generally 20-85 m thick and multiple sets of gas layers were developed and are considered as the main gas-bearing member in the Ordos Basin [28–30]. The whole Shan2 member is a monocline structure, which dips to the west, low to the west, and high to the east. The structure is simple, and the stratigraphic dip angle is less than 1°, with an average slope of about 2-8 m/km. The fold and fault structures are not well developed on the slope, and only low-amplitude nose-like uplift is developed. These nose-like uplift and sand bodies were almost superposed in the same position, effectively controlling the regional migration and accumulation of natural gas.

The Shanxi Formation stratum in the eastern Ordos Basin is a sea-land transition deposition. Alluvial plain, river, and residual shallow sea to lake delta depositional systems were developed from north to south [31, 32]. In the Shan2 phase, shallow sea delta deposition was developed as the early deposition of the Shanxi Formation. Provenance from the north was in plentiful supply, and sand bodies were widely distributed [33–35]. The sand bodies extended in a strip in the plane (Figure 1). The distributary channel is mainly composed of coarse, medium, and fine sandstones. The thickness of a single sand body is generally 4-8 m, and the cumulative thickness is 15-20 m. The ratio of sand to land is about 30%-60%, with the sand bodies showing apparent positive grain sequence bedding and regarded the most important gas-bearing sand bodies.

3. Samples and Research Methods

In this study, more than 180 core samples from 15 wells were collected, and more than 300 standard and cast thin rock sections were prepared. The characteristics of diagenesis and pore evolution and the influence of diagenesis on porosity were investigated based on petrographic observation. Content of cement, matrix, and porosity were counted separately and measured by a single operator.

The original porosity of sandstone was recovered by applying the original porosity calculation formula of isospheric particles proposed by Liu et al. [36]: the original porosity of clastic rock = 20.91 + 22.9/sorting coefficient (S). The remaining porosity after compaction was determined by the sum of the space occupied by cement in the current pores and the remaining intergranular pores after cementation, i.e., the remaining porosity after compaction (Q1, %) = the percentage of cement volume (Q2, %) + the remaining intergranular porosity (Q3, %).

Clay mineral analysis was carried out by D/MAX2500 X-ray diffractometer. Sandstone samples were soaked, precipitated, separated, and dried to obtain pure clay minerals in sandstone. X-ray diffraction analysis was performed to determine the type and relative content of clay minerals. JSM-7500F mode field emission scanning electron microscope (SEM), which has a secondary electron image resolution of 1 nm and magnification of 25~300 000 times, was used to characterize the structure and composition of sandstones, including cement, authigenic clays, and matrix. Core porosity and permeability tests were made on more than 2000 core plugs from 90 wells using standard techniques of oil and gas industry.

4. Results

4.1. Lithology. The lithology of the Shanxi Formation channel sand bodies in the eastern Ordos Basin is generally coarse to middle-grained sandstone, with medium roundness and sphericity of detrital particles. The statistical study of sandstone minerals under the microscope shows that the lithology of the gas-bearing layer in Shan2 member is mainly lithic sandstone and lithic quartz sandstone, followed by quartz sandstone (Figure 2). The quartz in lithic sandstone is generally 56%-70% in content, while the quartz has wavy extinction and metamorphic characteristics. The feldspar detritus content is typically less than 3.0%, and the majority is clay sized or carbonated, but its shape and cleavage are preserved. The rock debris consists primarily of flexible metamorphic rock debris, such as schist, phyllite, and mud slate, that has undergone obvious alteration and deformation (Figure 3). The sandstone structure is tight, with poorly developed primary pores and well-developed calcareous and siliceous cements, while the matrix is mainly clay and tuff, such as kaolinite, illite, and chlorite.

4.2. Diagenesis

4.2.1. Compaction. The main diagenetic processes identified by the petrology method from the samples are compaction, cementation, and dissolution. Microscopic observation shows that mica and plastic metamorphic rock cuttings such as slate and phyllite have been significantly deformed and distributed in a directional arrangement in lithic sandstone. Quartz particles are in close contact, showing mosaic contact boundaries and cracks (Figure 4). The degree of compaction is also different for different lithologies. For example, as heterobase content and detrital particle types differ, the bearable pressure of quartz and lithic sandstone and the degree of compaction are also different. According to the statistics of casting thin sections, the face rate of quartz sandstone and lithic sandstone is significantly different with different burial depths, and the decline rate of quartz sandstone is relatively low (Figure 5).

4.2.2. Cementation. The cementation of the sandstone is widely distributed and varying, including carbonate, clay minerals, and quartz cement. Carbonate cement includes authentogenic calcareous minerals such as calcite and iron dolomite. The results show that the calcite is red after staining, while iron-bearing dolomite cement is dark purple or blue-purple (Figures 6(a) and 6(b)). Electronic probe analysis shows that Fe of iron-bearing dolomite is 5.6%-12% in content. Microscopically, two generations of calcite cement can be identified: the early and late generations. The early

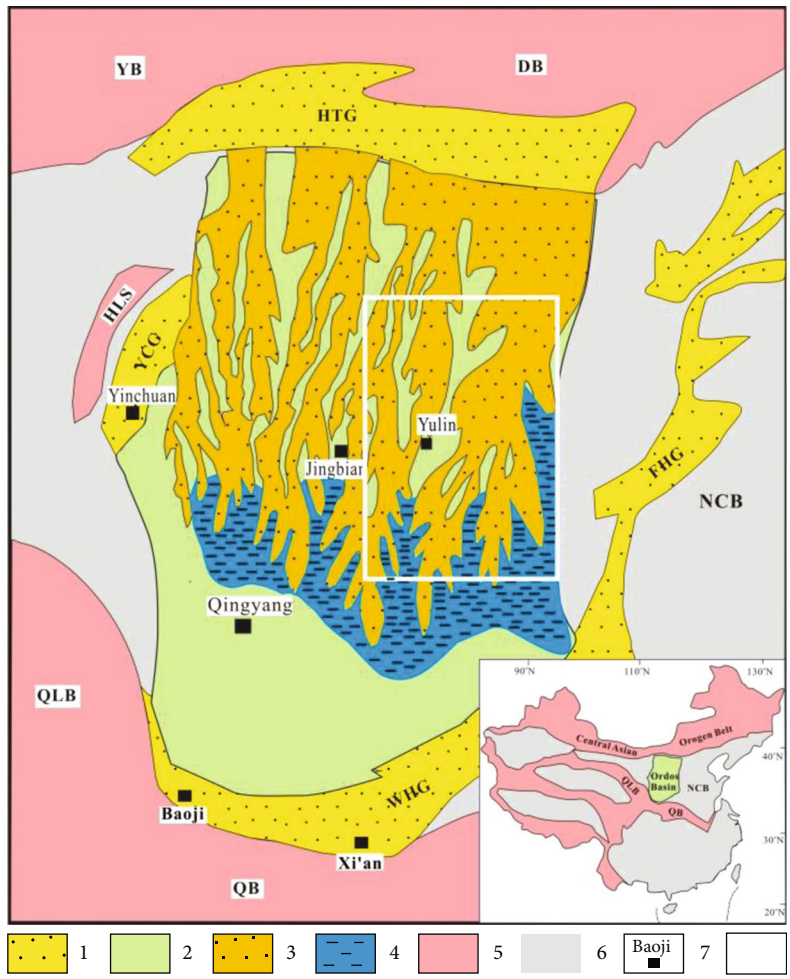

1-Cenozoic depression; 2-Delta flood plain; 3-Channel sand body;
4-Orogenic belt; 5-The North China block; 6-City; 7-Study area

YB-Yinshan orogenic belt; DB-Daqingshan orogenic belt; HLS-Helan shan orogenic belt;
QB-Qinling orogenic belt; QLB-Qilianshan orogenic belt; YCG-Yinchuan graben;
HTG-Hetao graben; FHG-Fenhe graben; NCB-North China block; SCB-South China block

Figure 1: Structure and sedimentary background of the Ordos Basin in the Early Permian.

generation is micrite, surrounded by the edge of detrital particles (Figure 6(b)), while the late generation is intergranular sparry calcite filled in intergranular pores with ferric dolomite. The late generation of calcite altered lithic fragment, feldspar, and kaolinite, whereas the early generation of carbonate minerals altered lithic fragment and feldspar the most.

According to the occurrence of late calcite cement and dolomite cements and the distribution of quartz enlargement edge, the formation of late calcite cements and dolomite cements is later than that of quartz secondary enlargement edge. The content of calcareous cements is generally between 1.2% and 5.6%, up to 12%, which is one of the main factors of porosity loss in sandstone.

The siliceous cement includes pore-filled siliceous cement, microcrystalline quartz cement, and the enlarged secondary edge of quartz. Pore-filling siliceous cement is distributed in intergranular pores, and its shape depends on the residual shape of intergranular pores (Figure 7(a)). The microcrystalline quartz grew from the surface of the clastic particles to the pores (Figure 7(b)), forming a comb shape around the clastic particles, with the microcrystalline quartz filled in the pores. Secondary enlarging edges of quartz usually grow along the edge of quartz particles and wrap the quartz particles in a ring shape with a width of up to 1 mm. The results show that multiple enlarging edges can be seen, and annular lines of clay films and layered matrix can be seen on the edge of some particles (Figure 7(c)).

Microscopic observation and X-ray diffraction analysis showed that the gas-bearing sandstone of the Shanxi Formation in the study area contains various types of clay minerals, mainly illite, kaolinite, illite/Mongolian mixed layer minerals, and chlorite. Illite is the highest content of 30.25-77.42%, followed by kaolinite of 11.22%-34.42% and Yi/Mongolian mixed layer of 4.7%-12.37%. The conversion degree of Yi/Mongolian mixed layer is high, and its mixed layer ratio (I/S) is 10%-15%. The chlorite content varies greatly, ranging from 2.2 to 19%, which is complementary

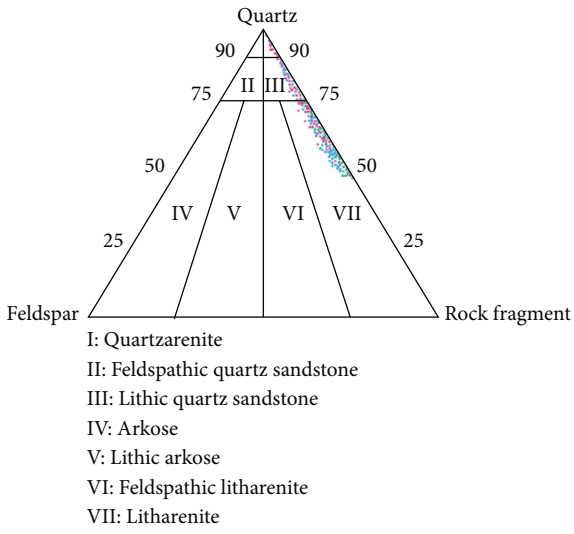

Figure 2: Classification of sandstone samples using Folk's classification (1974).

to illite content. With the increase of burial depth, the chlorite content decreases gradually and the illite content increases. Microscopically, abundant authigenic illite or illite/montmorillonite mixed layers are distributed around the detrital particles (Figure 8(a)). Illite is distributed as hair-like or fibrous particles under scanning electron microscopy (SEM). Part of the illite fibrous crystal is larger, mainly long flake, with a width of 1-2 μm and a length of up to 10 μm (Figure 8(b)). Chlorite and Yi/Mongolian mixed layer are observed as lamellar and are filled in pores with kaolinite. Kaolinites are subhedral six-party plate or anhedral crystal, generally 5-10 μm in size and distributed as aggregates (Figure 8(c)).

4.2.3. Alteration. The Shanxi Formation sandstone in the study area was clearly altered under the microscope (Figure 9). The metamorphic cuttings and feldspar detritus were clearly kaolinized, illitized, and carbonated. The two groups of cleavage and the shape of plate-columnar debris are still discernible after the feldspars were altered. In addition, the biotite and volcanic cuttings underwent illitization, while the clay, volcanic materials, and another complex matrix filling between the clastic particles underwent kaolinization.

4.2.4. Dissolution. The dissolution of the Shanxi Formation sandstone is strong. Mold pores form after feldspar, and rock debris are partially or entirely dissolved (Figure 10(a)). The cleavage and strip shape of feldspar can be identified after dissolution (Figure 10(b)). Although the unstable mica and feldspar were dissolved, the quartz remained in the metamorphic rock clast dissolution (Figure 10(c)). The residue around the pore can be used to identify the dissolution of cement, clay, and volcanic materials, and it is possible to recover the compositional characteristics prior to dissolution. The kaolinite altered by volcanic material was further dissolved to form secondary dissolution pores and intercrystalline pores. After calcite cement was dissolved, some calcite residues remained at the edge of the dissolution pores, and dolomite cement remained further after dissolution (Figure 10(d)).

4.3. Diagenetic Facies. Diagenetic facies, which have various petrological, diagenetic, and physical characteristics, are a comprehensive manifestation of sedimentary facies, lithology, and diagenesis [10, 14, 16]. Scholars classified diagenetic facies based on diagenesis, diagenetic environment, and pore characteristics [12–15]. Six different diagenetic facies have been identified in the Shanxi Formation based on petrographic observation, taking into account the types of rock, diagenesis, and pores and the degree of constructive diagenesis (dissolution, burst effect) and destructive diagenesis (compaction, cementation). These identified diagenetic facies are siliceous cementation intergranular pore facies, carbonate dissolution pore facies, matrix dissolution pore facies, clastic dissolution pore facies, matrix filling and strong compaction tight facies, and carbonate cementation and metasomatism tight facies (Table 1).

Siliceous cementation intergranular pore facies (diagenetic facies A) is dominated by quartz sandstone. Siliceous cementation and quartz secondary enlargement are well developed. Quartz particles come into close contact with one another, and the kaolinite intercrystalline pores and residual intergranular pores have developed to provide good pore connectivity and favorable petrophysical properties (Figure 11(a)). Carbonate dissolution pore facies (diagenetic facies B) is mainly composed of lithic quartz sandstone, with calcareous cement having good petrophysical properties and being mostly dissolved to form dissolution pores (Figure 11(b)). Matrix dissolution pore facies (diagenetic facies C) is mainly lithic sandstone and lithic quartz sandstone. However, the content of the matrix is high, which is dissolved to form dissolution pores (Figure 11(c)), and it is with good petrophysical properties. Clastic dissolution pore facies (diagenetic facies D) is mainly developed in lithic sandstone and lithic quartz sandstone. Clastics, feldspar, and kaolinite were all thoroughly dissolved (Figure 11(d)), with good physical characteristics. The lithic sandstones that make up the tight facies with matrix filling and strong compaction (diagenetic facies E) have a high matrix content that has been eroded into illite and kaolinite, among other minerals, and soft plastic debris that has been strongly compressed and deformed (Figure 11(e)). Additionally, the sandstones of this facies are dense, and the porosity and permeability are very low. Carbonate cementation and metasomatism tight facies (diagenetic facies F) are dominated mainly by lithic quartz sandstone and lithic sandstone, with a high content of calcareous cement and feldspar, when clastics are mostly carbonated. Calcareous cement basically fills primary pores, which have not been dissolved (Figure 11(f)). It is further indicated that this reservoir is dense and has poor petrophysical properties.

5. Discussion

5.1. Influence of Diagenesis on Petropetrophysical Properties of Tight Reservoir. Reservoir porosity and permeability are

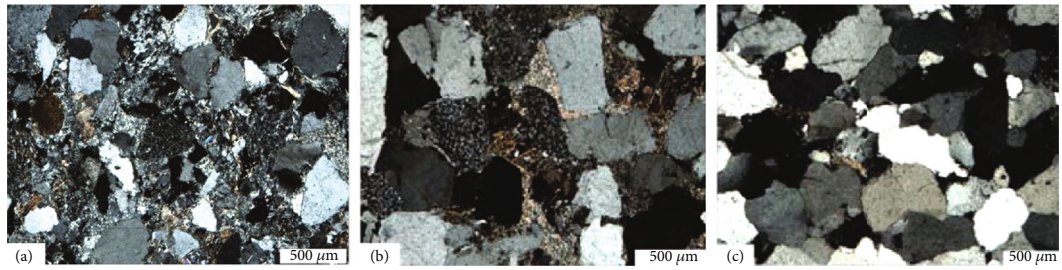

Figure 3: Photomicrographs show lithology characteristics of representative sandstone (plane polarized). (a) Lithic sandstone, showing most altered rock fragments, quartz, and feldspar grains with medium-grained and subangular. (b) Lithic quartz sandstone, showing altered rock fragments and quartz with medium-coarse-grained and subangular. (c) Quartz sandstone, showing quartz grains with medium and coarse grains and subangular.

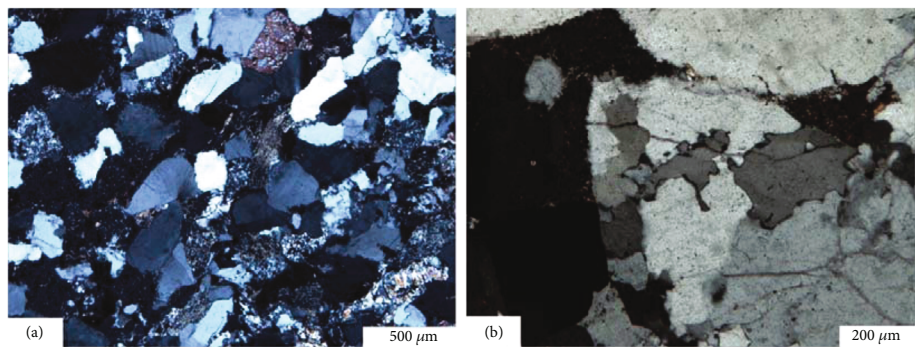

Figure 4: Photomicrographs show the compaction of representative sandstone (plane polarized).

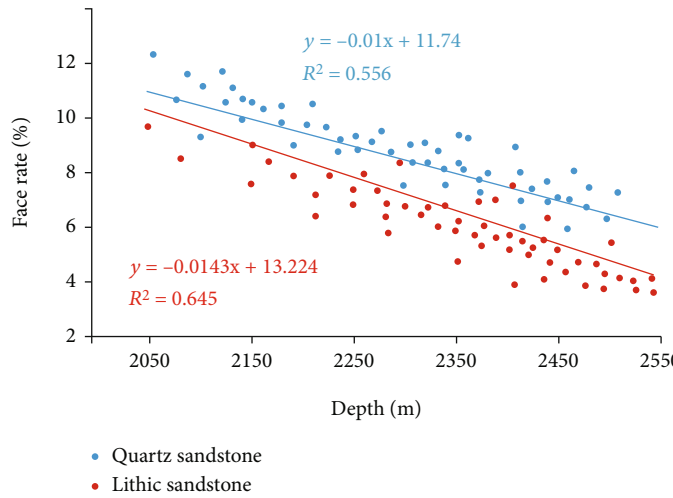

Figure 5: The relationship between burial depth and areal porosity of sandstones.

mainly controlled by its original sedimentation and the later process of diagenesis. The original porosities of different diagenetic facies are quite similar because they have different sedimentary facies, lithologies, rock structures, and diagenesis [37–39]. The original porosity was recovered by applying the Beard and Weyl quantitative analysis method [36], and the results revealed that the original porosity of sandstone ranged between 36.0% and 34.2% from the diagenetic facies A with the best petrophysical properties to the diagenetic facies F with the worst petrophysical properties. It is further demonstrated that the original porosity of various diagenetic facies is high and the original petrophysical properties are excellent, with no obvious different porosities of various diagenetic facies (Table 2) [40, 41]. As a result, the diagenesis after the sedimentary period should be the primary cause of the deterioration of the present petrophysical properties of sandstone with different diagenetic facies. The petrographic observation indicated

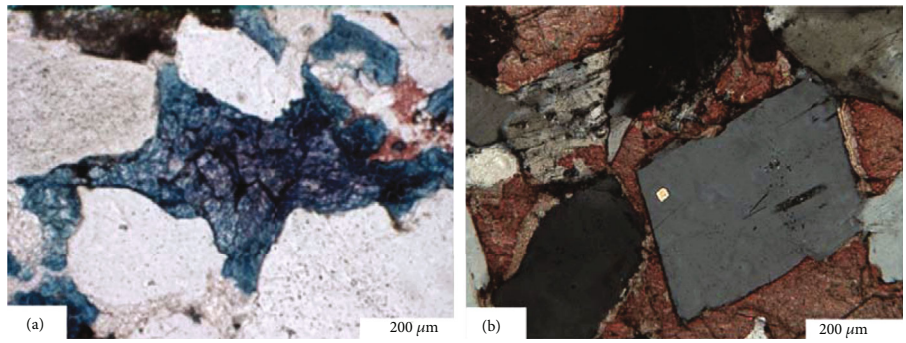

Dolomite cement with dyed blue engulfs quartz overgrowths and fills the intergranular pores.

Calcite cement of two phases, calcite I with dyed light red developed and circled around the detrital grains, and calcite II with dyed red filled the intergranular pores.

Figure 6: Photography of carbonate cement under the microscope.

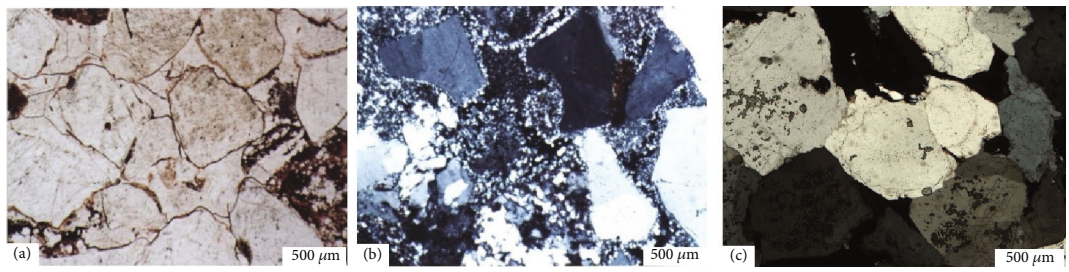

Figure 7: Siliceous cementation in sandstone.

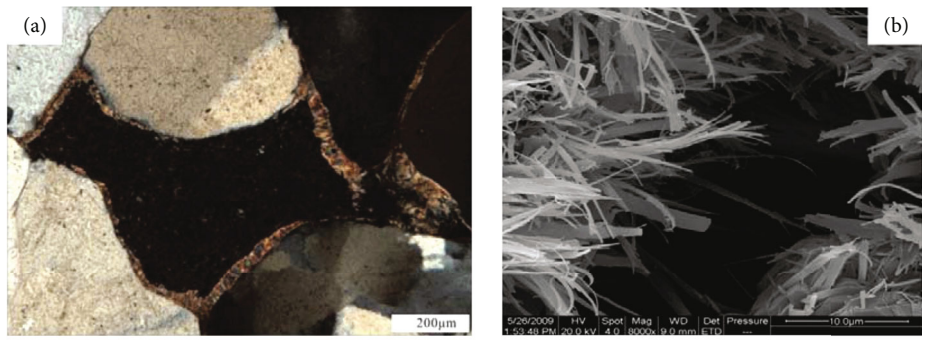

Distribution of illite-encrusting clastic particles under a polarizing microscope

Fibrous illite under scanning electron microscope

Aggregate of kaolinite, chlorite and illite

Aggregate of kaolinite

Figure 8: Occurrence of clay minerals in sandstone.

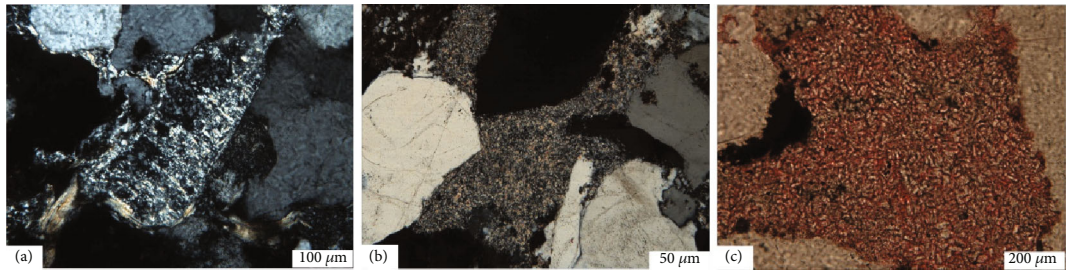

Figure 9: Sandstone alteration of the Shanxi Formation in study area.

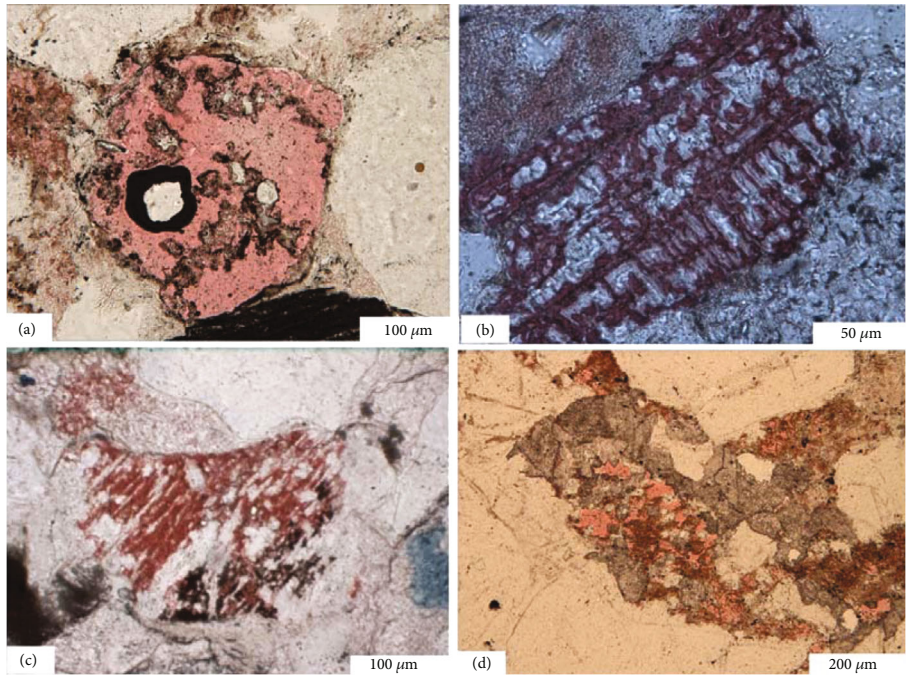

Figure 10: Dissolution pores of sandstone in the Shanxi Formation. (a) Casting pores of clastic particles. (b) Dissolution residue of plagioclase. (c) Dissolution of metamorphic rock debris (the residual siliceous minerals can be identified). (d) Residue after the dissolution of calcareous cement.

that the diagenetic sequence of sandstones in this area is compaction, cementation and alteration, dissolution, and later fissure.

5.1.1. Effect of Compaction on Petropetrophysical Properties of Different Diagenetic Facies. Compaction is the main factor leading to the loss of sandstone porosity [42, 43]. The microscopic observation indicated that most of the detritus particles were in line contact and that the debris had clearly deformed, with some parts being broken and pressure dissolved. Quantitative analysis revealed that the porosity lost by compaction of six different diagenetic facies is between 15.4% and 18.9%, and the residual porosity after compaction is between 20.6% and 15.3% (Table 2), indicating that the porosity of sandstone was still large after compaction, and the reservoir was not dense with a normal movement of natural gas. Therefore, compaction has different effects on the petrophysical properties of different diagenetic facies and is not the primary cause of reservoir compaction. In addition, diagenetic facies A has the highest quartz content, the strongest compaction resistance, the least porosity lost by compaction, and the highest residual porosity after compaction (Table 2). The surface porosity of quartz sandstone and lithic sandstone was quantitatively measured using the thin sections casting of sandstone and with different burial depths. It can be seen that with the increase of burial depth, quartz sandstone and lithic sandstone significantly decline with the rate of face, but the face rate drop of quartz sandstone is relatively small. When the burial depth is 2400 m, the face rate of quartz sandstone is about 9%, while the face rate of lithic sandstone at the same depth is only 3%.

5.1.2. Influence of Cementation on Petropetrophysical Properties of Different Diagenetic Facies. The cementation in the gas-bearing sandstone of the Shanxi Formation in the study area is very strong, mainly including siliceous, calcareous, and clay cementations. The results of the quantitative statistical analysis indicated that from diagenetic facies A with the

Table 1: Diagenetic facies of sandstone of research area.

Facies	Diagenetic facies	Diagenetic features	Pores	Rock types	
A	Siliceous cementation intergranular pore facies	Quartz enlargement, siliceous cement filling pores, kaolinite, pressure dissolution	Residual primary intergranular pores, intergranular pores of kaolinite	Quartz sandstone	
B	Carbonate dissolution pore facies	Strong dissolution of calcareous cement	Intergranular solution pores, mold pores	Lithic quartz sandstone, quartz sandstone	Constructive diagenesis
C	Matrix dissolution pore facies	Kaolinite, volcanic materials, and other matrix dissolved	Intergranular dissolved pores, intercrystalline dissolved pores, casting pores	Lithic sandstone, lithic quartz sandstone	
D	Clastic dissolution pore facies	Dissolution of clastics and feldspar	Intergranular solution pores, mold pores		
E	Matrix filling and strong compaction tight facies	High content of matrix, strong erosion and deformation of soft clastics	Pores not well developed	Lithic sandstone, lithic quartz sandstone	Destructive diagenesis
F	Carbonate cementation and metasomatism tight facies	High content of matrix and calcareous cement	Pores not well developed	Lithic sandstone	

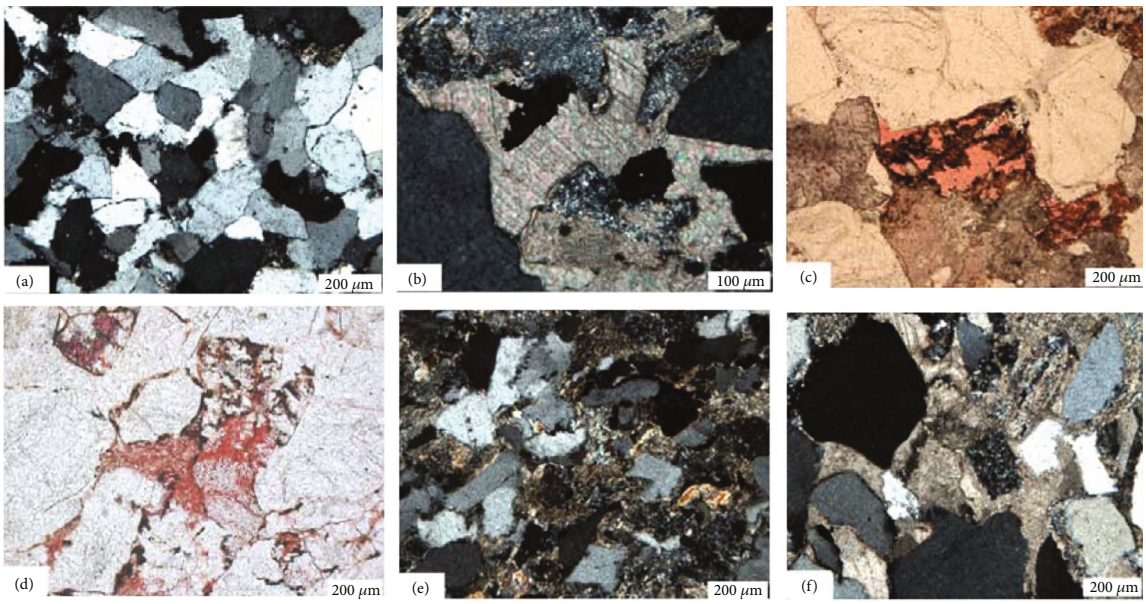

Figure 11: Photomicrographs of a representative sample from each diagenetic facies. (a) Diagenetic facies of siliceous cemented intergranular pores showing quartz sandstone, secondary growth of quartz, and development of siliceous cement and original residual pores. (b) Diagenetic facies of calcareous dissolution pores showing lithic sandstone and calcareous cement filled with intergranular pores is dissolved. (c) Diagenetic facies of mixed matrix dissolution pores showing detrital quartz sandstone, with the mixed matrix being all dissolved. (d) Cutting dissolution hole diagenetic facies showing detrital sandstone and flexible metamorphic rock cutting dissolution. (e) Strong compacted diagenetic facies of heterobasic alteration showing heterobasic alteration and strong deformation, with compacted dense structure. (f) Undissolved calcareous cementation metasomatism and dense diagenetic facies showing debris quartz sandstone with compacted structure and calcite cementation without dissolution.

best petrophysical properties to the diagenetic facies F with the worst petrophysical properties, the porosity loss caused by sandstone cementation was 11.9%-16.1%, and the residual porosity after cementation was only 8.7%-1.6% (Table 2). Porosity loss caused by cementation for different diagenetic facies was different, with the cementation having a minimal impact on porosity for diagenetic facies A. Furthermore, the porosity remains high even after cementation, which significantly impacts the interparticle porosity of diagenetic facies E and D, with less than 4.0% residual porosity after cementation. Petrography observation showed that they were mainly siliceous and authigenic clay cementation, resulting in tight reservoir formation. The relationship between the content of siliceous and calcareous cement and their petrophysical properties revealed that when the content of siliceous cement exceeds 4%, the change in porosity and permeability is

Table 2: Comparison of porosity evolution of sandstones of diagenetic facies.

Diagenetic facies	Original porosity (%)	Compacted porosity (%)		Cemented porosity (%)		Dissolution increases porosity (%)	Present porosity (%)	Permeability ($\times 10^{-3}$ μm^2)
		Loss	Remaining	Loss	Remaining			
A	36.0	15.4	20.6	11.9	8.7	0.3	9.0	0. 60
B	35.6	17.6	18.0	13.8	4.2	3.6	7.8	0.40
C	34.9	18.1	16.8	13.8	3.0	3.7	6.7	0.25
D	34.4	16.1	18.3	15.5	2.8	3.8	6.6	0.25
E	34.4	16.4	18.0	16.1	1.9	1.7	3.6	0.09
F	34.2	18.9	15.3	13.7	1.6	1.9	3.5	0.09
Average	34.9	17.1	17.8	14.1	3.7	2.5	6.2	0.21

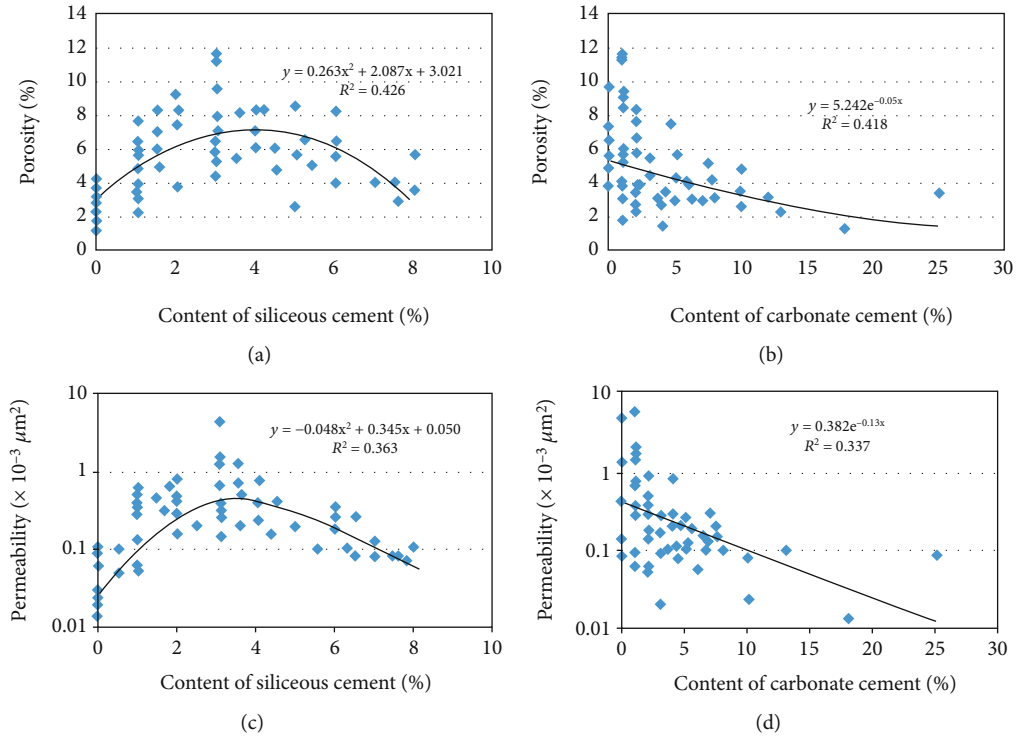

Figure 12: Relationship between cement content and petrophysical properties.

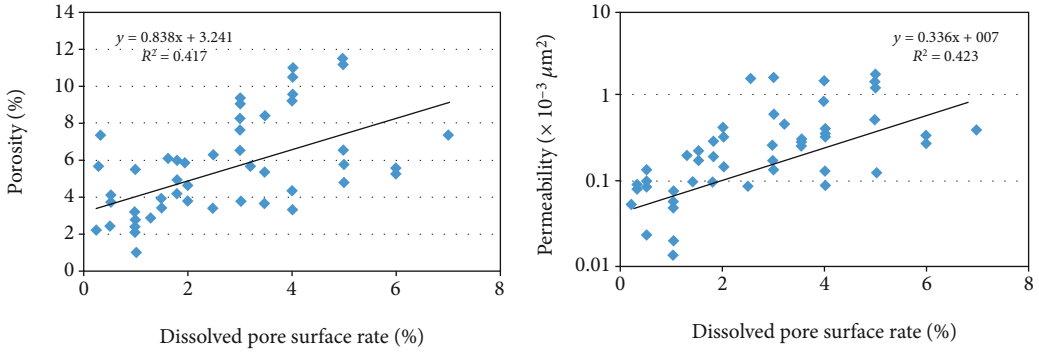

Figure 13: Relationship between dissolved pore surface rate and pore permeability.

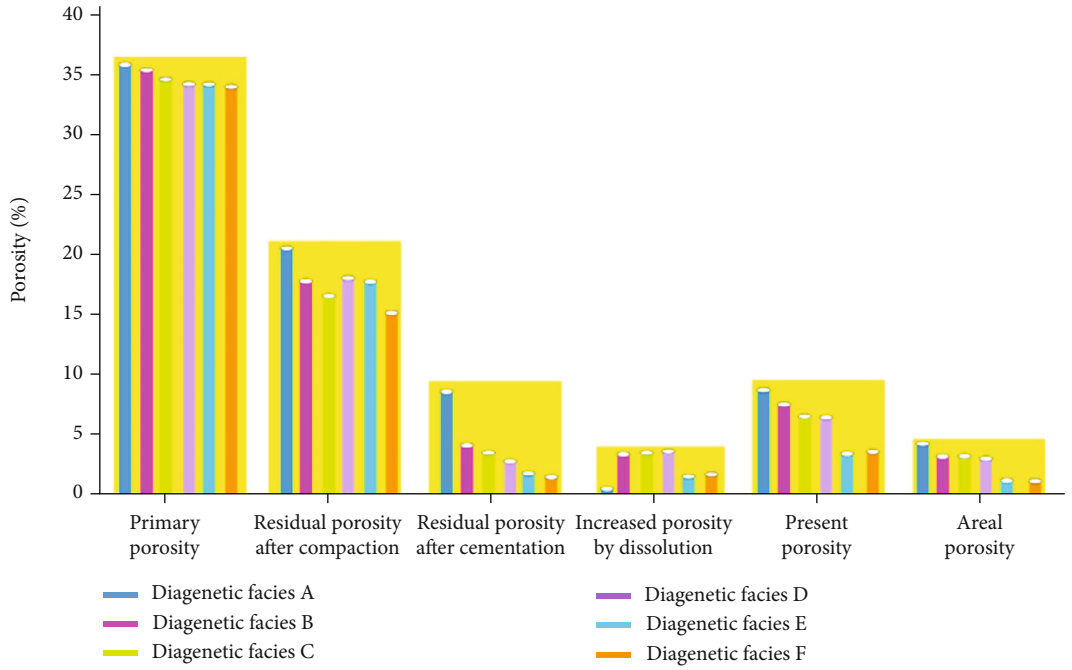

Figure 14: The porosity evolution process of different diagenetic facies in the Shanxi Formation.

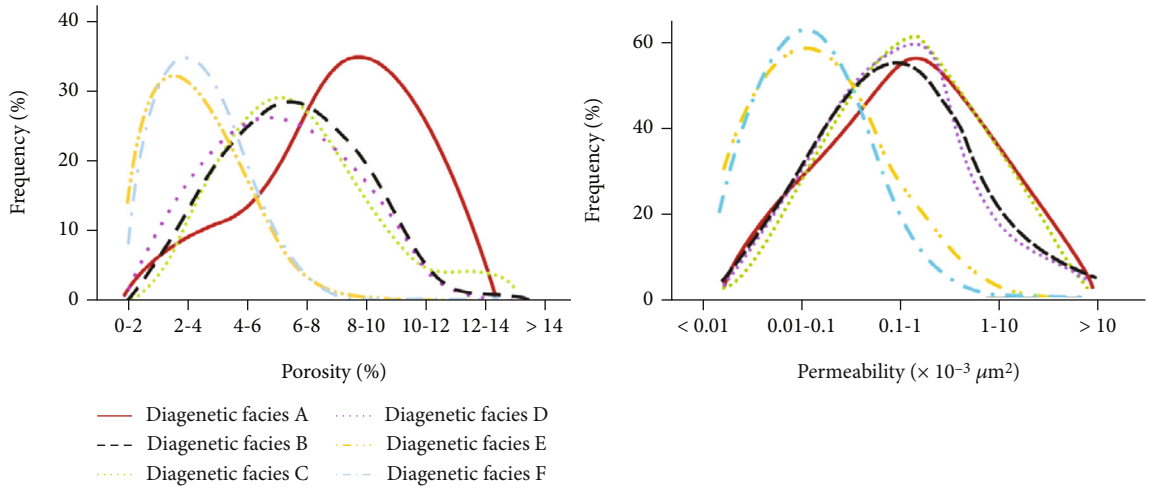

Figure 15: Porosity and permeability distribution of different diagenetic facies.

reversed; that is, porosity increases first and then decreases significantly. In contrast, carbonate cement will directly lead to the deterioration of petrophysical properties (Figure 12).

5.1.3. Improvement of Petrophysical Properties by Dissolution in Different Diagenetic Facies. The face rate of dissolution porosity is positively correlated with porosity and permeability (Figure 13). The present porosity of different diagenetic facies is generally 3.5%-9.0%, with an average of 6.2%, which is significantly higher than the remaining porosity after cementation (8.7%-1.6%) (Table 2). This is mainly due to the secondary porosity formed by late dissolution and fracturing. The new porosity increased by dissolution and fracturing was 0.3%-3.8% (Table 2). Among them, diagenetic facies B, C, and D improved significantly, and the increased porosity was 3.6%-3.8%, bringing the previous porosity of the tight reservoir (less than 4.0 percent) to 6.6%-7.8%. So the permeability of the reservoir is $(0.25 - 0.4) \times 10^{-3}\ \mu m^2$, which makes it an effective reservoir.

5.2. Impact of Diagenesis on the Petrophysical Properties of Different Diagenetic Facies. Different diagenesis has different impacts on the porosity of different diagenetic facies (Figure 14). The average porosity loss by compaction is 17.1% for all the diagenetic facies, and the average residual porosity after compaction is 17.8% (Table 2). After compaction, the reservoir porosity remains very high when compaction has the weakest effect on the petrophysical properties of diagenetic phase A (Figure 14). After compaction, the remaining primary intergranular pores are still well

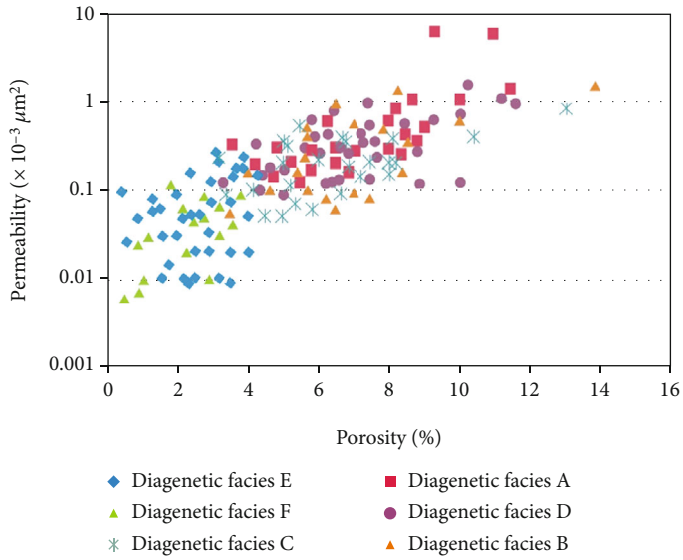

Figure 16: The correlation between porosity and permeability of different diagenetic facies.

developed, reaching up to 20.6%. This is because the diagenetic phase A is mainly quartz sandstone, with high content of rigid particles and strong compaction resistance. Porosity loss by cementation is averaging of 14.1%, but after cementation, the residual porosity is averaging of 3.7%. After cementation, phase A has a residual porosity of 8.7%, compared to less than 4.0% for the other phases, which are almost dense (Figure 14). Although the damage amplitude of cementation on the porosity of various diagenetic facies is less than that of compaction, it is evident that the reservoir becomes tight due to the cumulative influence of cementation. The porosity of diagenetic facies B, C, and D is increased by 3.6%-6.8%, with an average of 2.5%, due to the strong dissolution in the later stage. Among them, phases A, B, C, and D are effective reservoirs in this research area, with porosity greater than 6.6% and permeability of $(0.25 - 0.6) \times 10^{-3}\ \mu m^2$.

5.3. Influence of Diagenetic Facies on Reservoir Quality. Sandstone petrophysical parameters such as porosity and permeability are related to its original sedimentary characteristics and controlled by the later stages of diagenesis [44, 45]. For the porosity and permeability statistical results of different diagenetic facies (Figure 15), it can be seen that the petrophysical properties are obviously different [32, 46].

The porosity of diagenetic facies A is mainly between 6% and 12%, with a peak value of 8%-10% and an average value of 9.0% (Figure 15). However, the porosity distribution range of the sandstone diagenetic facies of B, C, and D is indicated to be between 4 and 10%, with a peak value of 6%-8% and an average value of 6%-8%, respectively, which is significantly lower than that of diagenetic facies A. For the sandstone diagenetic facies of E and F, it has the lowest petrophysical properties, with a distribution range of 2%-6% and a peak value of 3.5%.

The permeability of diagenetic facies A is between $(0.01 - 10) \times 10^{-3}\ \mu m^2$, with an average of $0.60 \times 10^{-3}\ \mu m^2$ and a peak value between $(0.1 - 1.0) \times 10^{-3}\ \mu m^2$. For the permeability of the diagenetic facies of B, C, and D, there is no significant difference from that of diagenetic facies A. Still, the distribution interval and peak value are slightly smaller. However, the permeability of the diagenetic facies of E and F is obviously small, with both less than $0.1 \times 10^{-3}\ \mu m^2$ (Figure 15).

Sandstone porosity and permeability have a good linear correlation, and permeability increases with the increase of porosity (Figure 16). However, the distribution characteristics of porosity and permeability are clearly different in various diagenetic facies. Diagenetic facies A and B have the best petrophysical properties, followed by diagenetic facies C and D, while the diagenetic facies E and F have the lowest petrophysical properties and the smallest porosity and permeability (Figure 16). Therefore, the diagenetic facies E and F have the worst petrophysical properties and are nonreservoirs. From the above discussion, the diagenetic facies A and B reservoirs have the best quality, and their distribution areas are the favorable exploration areas.

6. Conclusion

(1) Six types of diagenetic facies were identified in the Upper Paleozoic gas-bearing tight reservoir in the eastern Ordos Basin, which are in large differences in petrophysical properties. Diagenetic facies A is the best reservoirs being mainly of primary intergranular pores, and diagenetic facies B, C, and D are also effective reservoirs being mainly of secondary dissolution pore while diagenetic facies E and F are regarded as nonreservoir

(2) The restored original porosity is between 34.2% and 36.0% for all kinds of diagenetic facies. The average porosity loss by compaction is 17.1%, and the average porosity loss due to cementation is 14.1%. The porosity was increased by dissolution in the late stage by 2.5%. The average porosity loss by

compaction is low in diagenetic facies A, and the porosity increased by dissolution is high in diagenetic facies B, C, and D

(3) The distribution areas of diagenetic A, B, C, and D, with the porosity and permeability averaging of 6.6%-9.0% and $(0.25 - 0.6) \times 10^{-3}\ \mu m^2$, respectively, are favorable areas for tight gas exploration and are important indicators for the prediction of tight gas in the Upper Paleozoic Shanxi Formation in the eastern Ordos Basin

Data Availability

Data is available on request.

Conflicts of Interest

The authors declare no conflicts of interest.

Acknowledgments

This study was funded by the National Natural Science Foundation of China (no. 42273064 and no. 42202160), the Natural Science Foundation of Shandong Province (no. ZR2021QD057), the Scientific and Technological Innovation Programs of Higher Education Institutions in Shanxi (no. 2021L590), and the Fundamental Research Funds for the Central Universities, Chang'an University (no. 300102270109).

References

[1] C. Zou, G. Zhai, G. Zhang et al., "Formation, distribution, potential and prediction of global conventional and unconventional hydrocarbon resources," *Petroleum Exploration and Development*, vol. 42, no. 1, pp. 13–25, 2015.

[2] C. Zou, Q. Zhao, H. Wang et al., "Theory and technology of unconventional oil and gas exploration and development helps China increase oil and gas reservers and production," *Petroleum Science and Technology Forum*, vol. 40, no. 3, pp. 72–79, 2021.

[3] L. Sun, C. Zou, A. Jia et al., "Development characteristics and orientation of tight oil and gas in China," *Petroleum Exploration and Development*, vol. 46, no. 6, pp. 1015–1026, 2019.

[4] J. Dai, Y. Ni, and X. Wu, "Tight gas in China and its significance in exploration and exploitation," *Petroleum Exploration and Development*, vol. 39, no. 3, pp. 257–264, 2012, (in Chinese with English Abstract).

[5] X. Zhu, R. Pan, S. Zhu, W. Wei, and L. Ye, "Research progess and core issues in tight reservoir exploration," *Earth Science Frontiers*, vol. 25, no. 2, pp. 141–146, 2018.

[6] S. Henares, L. Caracciolo, C. Viseras, J. Fernandez, and L. M. Yeste, "Diagenetic constraints on heterogeneous reservoir quality assessment: a Triassic outcrop analog of meandering fluvial reservoirs," *AAPG Bulletin*, vol. 100, no. 9, pp. 1377–1398, 2016.

[7] H. Huang, R. Li, F. Xiong et al., "A method to probe the pore-throat structure of tight reservoirs based on low-field NMR: insights from a cylindrical pore model," *Marine and Petroleum Geology*, vol. 117, no. 104344, p. 104344, 2020.

[8] K. Xi, Y. Cao, J. Jahren et al., "Diagenesis and reservoir quality of the Lower Cretaceous Quantou formation tight sandstones in the southern Songliao basin, China," *Sedimentary Geology*, vol. 330, no. 1, pp. 90–107, 2015.

[9] R. Li, L. Duan, S. Zhang, B. Chen, B. Shi, and G. Yan, "Review on oil/gas accumulation with low permeability in Ordos basin," *Journal of Earth Science and Environment*, vol. 33, no. 4, pp. 364–372, 2011, (in Chinese with English Abstract).

[10] A. A. Mostafa, A. A. Khadrah, and A. A. Refaat, "Impact of diagenesis on reservoir quality evolution of the late Cenomanian Abu Roash "G" member in the Sitra field, North Western Desert, Egypt," *Marine and Petroleum Geology*, vol. 9, no. 5, pp. 255–264, 2018.

[11] H. Huang, R. Li, W. Chen et al., "Revisiting movable fluid space in tight fine-grained reservoirs: a case study from Shahejie shale in the Bohai Bay basin, NE China," *Journal of Petroleum Science & Engineering*, vol. 207, no. 109170, p. 109170, 2021.

[12] C. Zou, S. Tao, H. Zhou et al., "Genesis, classification and evaluation method of diagenetic facies," *Petroleum Exploration and Development*, vol. 35, no. 5, pp. 46–54, 2008.

[13] J. Lai, G. Wang, S. Wang, Y. Zheng, H. Wu, and Y. Zhang, "Research status and advances in the diagenetic facies of clastic reservoirs," *Advances in Earth Science*, vol. 28, no. 1, pp. 39–50, 2013.

[14] J. Lai, G. Wang, S. Wang et al., "Review of diagenetic facies in tight sandstones: diagenesis, diagenetic minerals, and prediction via well logs," *Earth-Science Reviews*, vol. 18, no. 5, pp. 234–258, 2018.

[15] J. Fu, "Accumlation characteristics and exploration potencial of gight limestone gas in the Taiyuan formation of the Ordos basin," *Earth Science Frontiers*, vol. 30, no. 1, pp. 20–29, 2023, (in Chinese with English Abstract).

[16] X. Guo, D. Zhou, P. Zhao, Z. Liu, D. Zhang, and D. Feng, "Progresses and directions of unconventional natural gas exploration and development in the Carboniferous-Permian coal measure strata, Ordos basin," *Oil & Gas Geology*, vol. 43, no. 5, pp. 1013–1023, 2022, (in Chinese with English Abstract).

[17] D. Liu, W. Zhang, Q. Kong, Z. Fen, C. Fang, and W. Peng, "The source rocks of Lower Paleozoic and natural gas causes in the Ordos basin," *Petroleum Exploration and Development*, vol. 43, no. 4, pp. 540–549, 2016.

[18] Y. Li, A. Fan, R. Yang, Y. Sun, and N. Lenhardt, "Sedimentary facies control on sandstone reservoir properties: a case study from the Permian Shanxi formation in the southern Ordos basin, Central China," *Marine and Petroleum Geology*, vol. 129, pp. 1–16, 2021.

[19] H. Huang, R. Li, Z. Lyu et al., "Comparative study of methane adsorption of Middle-Upper Ordovician marine shales in the western Ordos basin, NW China: insights into impacts of moisture on thermodynamics and kinetics of adsorption," *Chemical Engineering Journal*, vol. 446, no. 137411, p. 137411, 2022.

[20] A. Ozkan, S. P. Cumella, K. L. Milliken, and S. E. Laubach, "Prediction of lithofacies and reservoir quality using well logs, Late Cretaceous Williams Fork formation, Mamm Creek field, Piceance basin, Colorado," *AAPG Bulletin*, vol. 95, no. 10, pp. 1699–1723, 2011.

[21] G. A. Oluwadebi, K. G. Taylor, and P. J. Dowey, "Diagenetic controls on the reservoir quality of the tight gas Collyhurst sandstone formation, Lower Permian, East Irish Sea Basin,

United Kingdom," *Sedimentary Geology*, vol. 371, pp. 55–74, 2018.

[22] H. Huang, R. Li, Z. Jiang, J. Li, and L. Chen, "Investigation of variation in shale gas adsorption capacity with burial depth: insights from the adsorption potential theory," *Journal of Natural Gas Science & Engineering*, vol. 73, p. 103043, 2020.

[23] J. Wang, Y. Cao, K. Liu, J. Liu, and M. Kashif, "Identification of sedimentary-diagenetic facies and reservoir porosity and permeability prediction: an example from the Eocene beach-bar sandstone in the Dongying depression, China," *Marine and Petroleum Geology*, vol. 82, pp. 69–84, 2017.

[24] W. J. Al-Mudhafar, "Integrating well log interpretations for lithofacies classification and permeability modeling through advanced machine learning algorithms," *Journal of Natural Gas Science and Engineering*, vol. 7, pp. 1023–1033, 2017.

[25] J. J. Stuart, Z. Zhou, J. Lai, Y. Cui, and G. Wang, "Prediction of diagenetic facies using well logs-a case study from the upper Triassic Yanchang formation, Ordos basin, China," *Marine and Petroleum Geology*, vol. 81, pp. 50–65, 2017.

[26] H. Liu, Y. Zhao, Y. Luo, Z. Chen, and S. He, "Diagenetic facies controls on pore structure and rock electrical parameters in tight gas sandstone," *Journal of Geophysics and Engineering*, vol. 12, no. 4, pp. 587–600, 2015.

[27] Y. Ran, G. Wang, J. Lai et al., "Quantitative characterization of diagenetic facies by using logging cross plot: a case study on Chang 7 tight sandstone oil reservoir in Heshui area, Ordos basin," *Acta Sedimentological Sinica*, vol. 34, no. 4, pp. 694–706, 2016, (in Chinese with English Abstract).

[28] J. Wang, Y. Cao, K. Liu, A. Costanzo, and M. Feely, "Diagenesis and evolution of the lower Eocene red-bed sandstone reservoirs in the Dongying depression, China," *Marine and Petroleum Geology*, vol. 94, pp. 230–245, 2018.

[29] R. Li and Y. Li, "Tectonic evolution of the western margin of the Ordos basin (Central China)," *Russian Geology and Geophysics*, vol. 49, no. 1, pp. 23–27, 2008.

[30] S. Li, G. Zhao, L. Dai et al., "Mesozoic basins in eastern China and their bearing on the deconstruction of the North China Craton," *Journal of Asian Earth Sciences*, vol. 47, no. 30, pp. 64–79, 2012.

[31] S. Liu, "The coupling mechanism of basin and orogen in the western Ordos basin and adjacent regions of China," *Journal of Asian Earth Science*, vol. 16, no. 4, pp. 369–383, 1998.

[32] Y. Yang, W. Li, and L. Ma, "Tectonic and stratigraphic controls of hydrocarbon systems in the Ordos basin: a multicycle cratonic basin in Central China," *AAPG Bulletin*, vol. 89, no. 2, pp. 255–269, 2005.

[33] D. Liu, W. Zhang, Q. Kong, Z. Feng, C. Fang, and W. Peng, "Lower Paleozoic source rocks and natural gas origins in Ordos basin, NW China," *Petroleum Exploration & Development*, vol. 43, no. 4, pp. 591–601, 2016.

[34] H. Yang, J. Fu, and X. Wei, "Characteristic of natural gas reservoir formation in Ordos basin," *Natural Gas Industry*, vol. 25, no. 4, pp. 5–8, 2005, (in Chinese with English Abstract).

[35] W. Wang, P. Liu, L. Zheng, X. Zhou, and S. Jiang, "Natural gas reserves and production prediction of Ordos basin," *Natural Gas Geoscience*, vol. 25, no. 9, pp. 1483–1490, 2014, (in Chinese with English Abstract).

[36] F. Liu, R. Li, X. Liu et al., "Study of gas accumulation under "source control"in western Sulige gas field, Ordos basin," *Acta Sedimentologica Sinica*, vol. 37, no. 6, pp. 1129–1139, 2019, (in Chinese with English Abstract).

[37] H. Yang, X. Liu, and X. Yan, "Tectonic-sedimentary evolution and tight sandstone gas accumulation in Ordos basin since Late Paleozoic," *Earth Science Frontiers*, vol. 22, no. 3, pp. 174–183, 2015, (in Chinese with English Abstract).

[38] H. Yang, X. Liu, X. Yan, and H. Zhang, "The Shenmu gas field in the Ooros basin: its discovery and reservoir-forming geological characteristics," *Natural Gas Industry*, vol. 39, pp. 8–20, 2015, (in Chinese with English Abstract).

[39] K. Xi, Y. Cao, K. Liu et al., "Diagenesis of tight sandstone reservoirs in the upper Triassic Yanchang formation, southwestern Ordos basin, China," *Marine and Petroleum Geology*, vol. 99, pp. 548–562, 2019.

[40] X. Wang and C. Mou, "Diagenesis and diagenetic facies of reservoir in He 8 section of Shihezi formation in east II part of Sulige gas field," *Natural Gas Geoscience*, vol. 24, no. 4, pp. 678–689, 2013, (in Chinese with English Abstract).

[41] M. Ingrid, "Petroleum inclusions in sedimentary basins: systematics, analytical methods and applications," *Lithos*, vol. 55, no. 1–4, pp. 195–212, 2001.

[42] X. Sun, J. Wang, C. Tao et al., "Geochemical characteristics and source of Paleozoic natural gas in Daniudi, Ordos basin," *Acta Petrolei Sinica*, vol. 43, no. 2, pp. 307–314, 2021, (in Chinese with English Abstract).

[43] D. C. Beard and P. K. Weyl, "Influence of texture on porosity and permeability in unconsolidated sand," *AAPG Bulletin*, vol. 57, no. 2, pp. 349–369, 1973.

[44] T. Lei, H. Deng, D. Wu et al., "Depositional model of the lower-middle Ordovician Majiagou formation in Daniudi gas field, Ordos basin," *Journal of Palaeogeography*, vol. 22, no. 3, pp. 523–538, 2020, (in Chinese with English Abstract).

[45] J. Fu, X. Wei, S. Luo et al., "Discovery and geological understanding of Qingyang deep coal-derived gas field," *Petroleum Exploration and Development*, vol. 46, no. 6, pp. 1047–1061, 2019.

[46] Z. Ren, S. Zhang, S. Gao, J. Cui, Y. Xiao, and H. Xiao, "The tectonic thermal evolution history of Ordos basin and its significance of accumulation and mineralization," *Scientia Sinica (Terrae)*, vol. 37, no. S1, pp. 23–32, 2007.